ACS OMEGA

Open Access

http://pubs.acs.org/journal/acsodf

Article

Electrostatic Nanocage-Confined Probe for Electrochemical Detection of CA19-9 in Human Serum

Yucheng Zhou, Xuan Luo, Fei Yan,* and Yiping Mou*

Cite This: *ACS Omega* 2023, 8, 48491−48498

Read Online

ACCESS | Metrics & More | Article Recommendations | Supporting Information

ABSTRACT: Prompt and accurate detection of CA19-9 in human serum has great clinical significance for the early diagnosis and disease monitoring of cancer. Herein, we develop a convenient and antifouling electrochemical sensor for CA19-9 determination by immobilization of both an electrochemical redox probe [methylene blue (MB)] and immunorecognition element (CA19-9 antibody) on an electrostatic nanocage consisting of bipolar silica nanochannel array (bp-SNA). bp-SNA is composed of a negatively charged inner layer (n-SNA) and positively charged outer layer (p-SNA), which could be stably prepared on indium tin oxide (ITO) in several seconds using a two-step electrochemically assisted self-assembly approach and display asymmetric surface charges for confinement and enrichment of cationic MB into the inner n-SNA layer through electrostatic interaction. Modification of the CA19-9 antibody on the top surface of bp-SNA confers the sensing interface with specific recognition capacity. An antibody−antigen complex formed at the as-prepared immunosensor causes the decreased electrochemical signals of MB, achieving sensitive determination of CA19-9 with a wider linear dynamic range from 10 μU/mL to 50 U/mL and a low detection limit (3 μU/mL). Furthermore, accurate and feasible analysis of the CA19-9 amount in human serum samples by our proposed probe-integrated electrochemical immunosensor is realized.

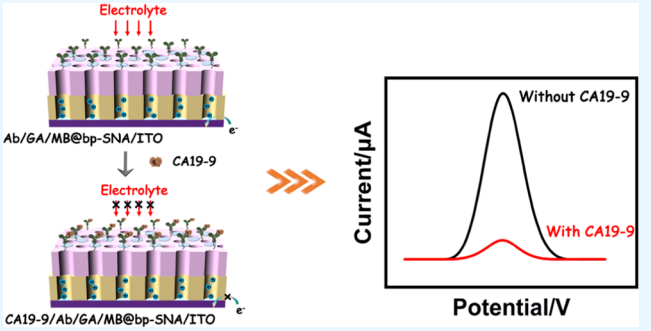

1. INTRODUCTION

Highly sensitive and fast determination of tumor-related biomarkers is essential for early diagnosis, disease monitoring, and accurate prediction of cancer.[1] Carbohydrate antigen 19-9 (CA19-9), a carbohydrate antigen consisting of macromolecular glycoproteins, is one of the most crucial tumor biomarkers associated with many malignant tumors such as pancreatic, colorectal, liver, gastric, and ovarian,[2,3] which exhibits great clinical significance. Although CA19-9 can be present in the blood of normal healthy people at a very low amount (usually less than 37 U/mL), its amount will increase dramatically in cancer patients.[4] To date, techniques for the quantitative detection of CA19-9 include enzyme-linked immunosorbent assay (ELISA),[5] photoluminescence,[6] and electrochemiluminescence (ECL).[7] These assays have many advantages but also have some drawbacks, such as large sample volume, complicated and expensive instruments, and limited sensitivity. Recently, electrochemical immunosensors have attracted great interest owing to their features of simple devices, low cost, high sensitivity, and easy miniaturization.[8−12]

Vertically ordered mesoporous silica films [also termed as silica nanochannel array (SNA)] are a kind of synthetic nanoporous membrane with selective permeability and controlled molecular transport, which enable the design of a vast variety of novel electrochemical/electrochemiluminescent sensors.[13−18] Their unique characteristics with respect to the ultrasmall and uniform diameter of silica pores, ultrathin, high porosity, and insulated property especially offer a broad prospect for the direct analysis of complicated biological samples.[19−21] Analytes with redox-active characteristic can be directly determined based on their electrochemical signals on the SNA-based sensors.[22,23] As for the tumor biomarkers without electroactive property, both recognition elements and probes are employed and the target-introduced large complex on the outer surface of SNA leads to the signal variation of free electrochemical/ECL probes in solution or electrochemical/ECL probes immobilized on the SNA-based sensors and further realizes their quantitative determination.[24−26] In contrast, probes immobilized into the nanochannels of SNA offer advantages of easy detection operations, sparing chemical reagents, and low cost without the addition of exogeneous reagents. Su's group has reported a nanocage consisting of SNA bilayers with different pore diameters for physical trapping ECL probe (tris(4,7-diphenyl-1,10-phenanthroline)-

Received: October 24, 2023
Revised: November 6, 2023
Accepted: November 14, 2023
Published: December 4, 2023

Scheme 1. Illustration for the Fabrication of bp-SNA/ITO (a), MB@bp-SNA/ITO-Based Immunosensor (b), and Its Electrochemical Sensing Mechanism for CA19-9 (c)[a]

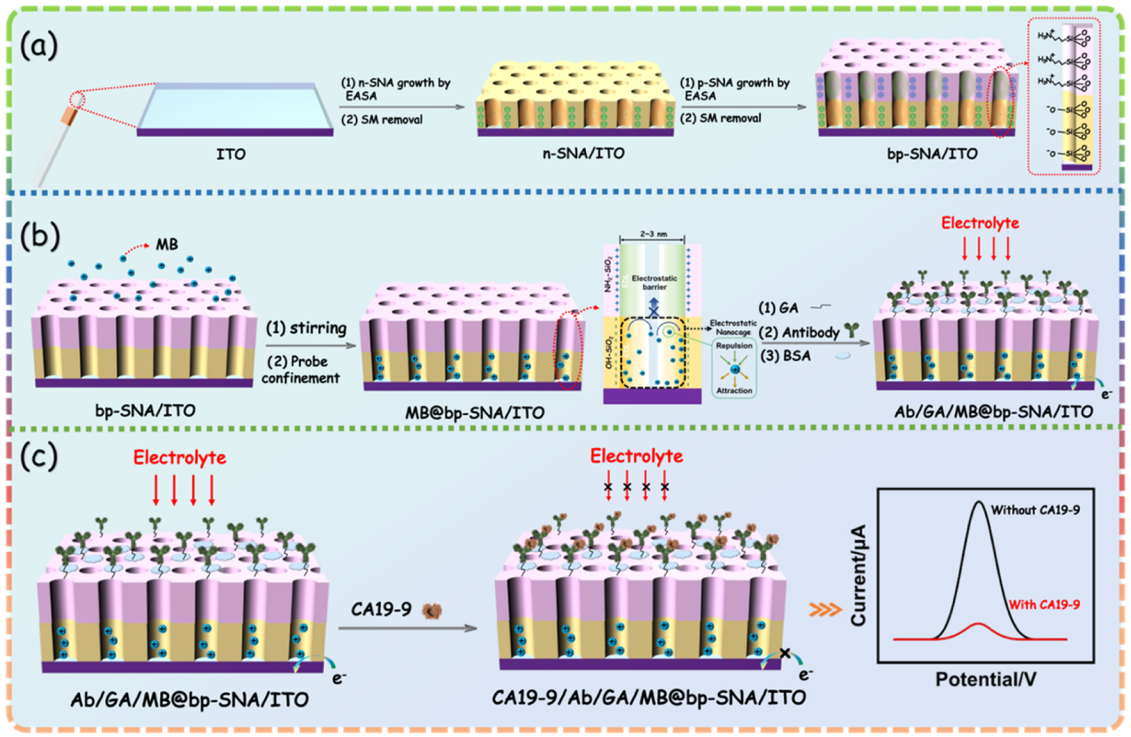

[a]The area of the tested MB@bp-SNA/ITO-based immunosensor is 0.5 cm^2.

ruthenium(II) dichloride), allowing the determination of dopamine released from living PC cells based on the quenching effect.[27] This bilayer SNA nanocage process is performed by using the biphasic-stratification growth method and poly(methylmethacrylate)-assisted transfer approach, which however requires professional technicians and several complicated steps. Our group has recently prepared a bilayer SNA carrying asymmetric surface charges using a simple and prompt electrochemically assisted self-assembly (EASA) method, which can further act as an electrostatic cage for confinement of the tris(2,2′-bipyridyl)ruthenium(II) ECL probe and apply to detect disease-related biomarkers (e.g., SARS-CoV-2 IgG antibody),[28] carcinoembryonic antigen (CEA), and carcinoma antigen 15-3 (CA15-3).[29]

Methylene blue (3,7-bis(dimethylamino)-phenothiazin-5-ium chloride, abbreviated as MB) is an electrochemically active cationic thiazine dye, which has widely been used for the fabrication and design of electrochemical sensors.[30] In this work, an electrostatic nanocage consisting of a bipolar silica nanochannel array (bp-SNA) is prepared on the indium tin oxide (ITO) electrode surface in several seconds by using a two-step EASA method, which shows asymmetric surface charges and is used for confinement and enrichment of MB molecules into the inner tiny layer of bp-SNA through electrostatic effect. Such MB immobilized into the bp-SNA-modified ITO electrode can be then designed as the convenient electrochemical immunosensor for CA19-9 determination with low cost and high sensitivity. The inner and outer layers of bp-SNA carry negative and positive charges, namely, n-SNA and p-SNA, providing dual electrostatic force toward cationic MB molecules to generate a stable and amplified electrochemical signal. Functionalization with CA19-9 antibody on the top surface of bp-SNA confers the sensing electrode with high specificity, and immune recognition formed on the sensing interface enables quantification of CA19-9. Direct analysis of the CA19-9 amount in human serum is also evaluated, and satisfactory results are obtained. Our proposed strategy immobilizes both the redox-active probe and recognition element onto the solid bp-SNA, sparing the usage of chemicals and improving the analytical sensitivity.

2. EXPERIMENTAL SECTION

Experimental sections including chemicals and instruments used in this study, synthesis of the MB@bp-SNA/ITO-based electrochemical immunosensor, and quantitative analysis of CA19-9 using the differential pulse voltammetry (DPV) technique are provided in the Supporting Information in detail.

3. RESULTS AND DISCUSSION

3.1. Fabrication of the MB@bp-SNA/ITO-Based Immunosensor. Scheme 1 illustrates the preparation process of the MB@bp-SNA/ITO electrode and its application for designing the CA19-9-specific sensing interface. Two-layer SNA with opposite surface charge is first grown onto the ITO surface using a two-step EASA method and changing the composition of the silica-based precursor according to our previous report.[31] n-SNA near the underlying ITO electrode bears a negatively charged surface, and p-SNA near the bulk solution carries a positively charged surface, which together constitute an electrostatic cage, namely, bp-SNA. MB molecules with positive charge can enter the p-SNA layer by vigorous mechanical stirring and be electrostatically confined into the silica nanochannels of n-SNA. In such a case, p-SNA positioned on the outer layer also can prevent the leakage of confined MB molecules from the inner layer through an

https://doi.org/10.1021/acsomega.3c08370
ACS Omega 2023, 8, 48491−48498

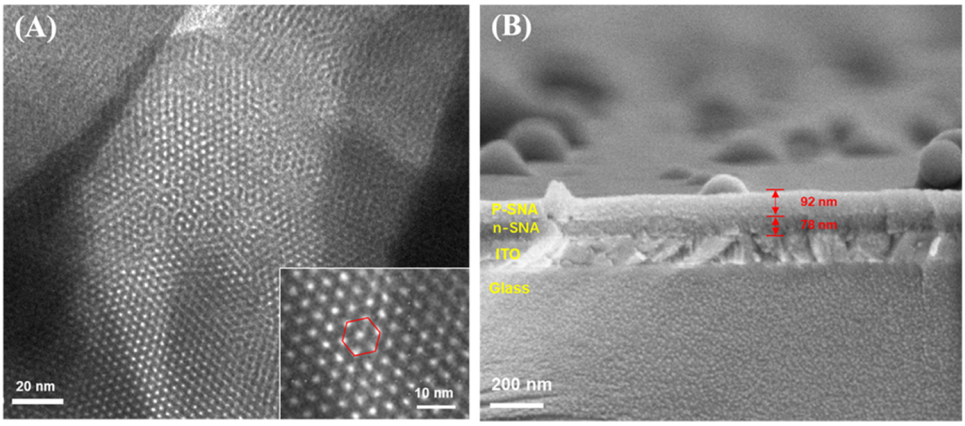

Figure 1. (A) Top-view TEM image of bp-SNA. The inset is the amplified image; (B) Cross-sectional view SEM image of bp-SNA/ITO.

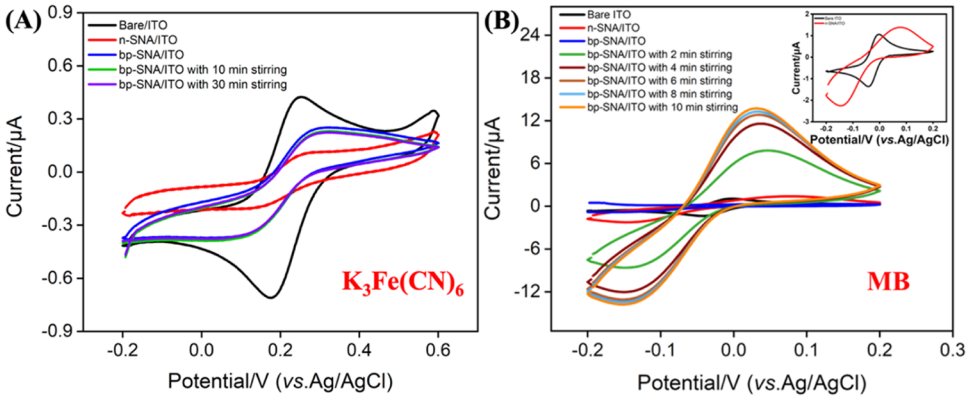

Figure 2. Cyclic voltammetry (CV) responses of bp-SNA/ITO, n-SNA/ITO, and bare ITO electrodes to (A) 10 μM $K_3Fe(CN)_6$ and (B) MB in a KHP solution (0.05 M, pH = 4) at a scan rate of 50 mV/s. The inset in (B) is the magnified CV curves of bare ITO and n-SNA/ITO electrodes.

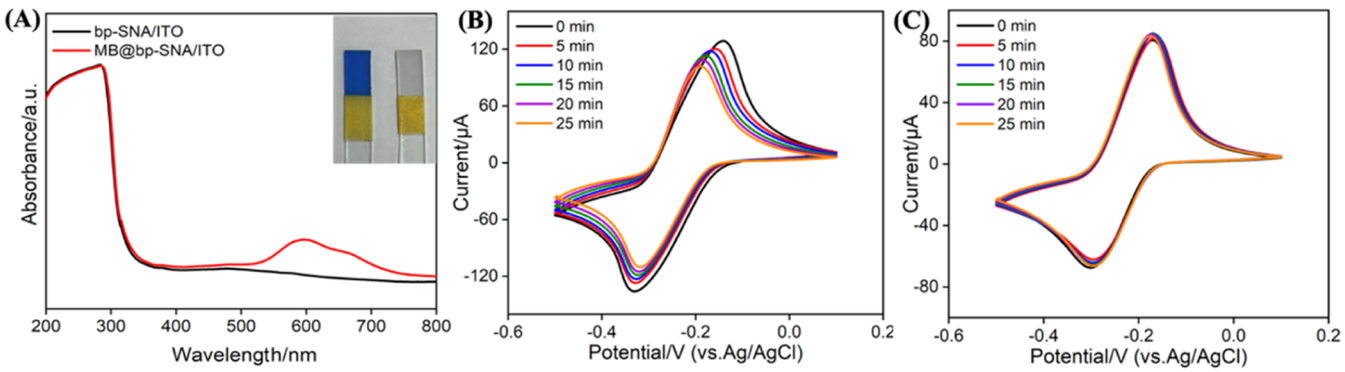

Figure 3. (A) UV−vis spectra of bp-SNA/ITO before and after the immobilization of MB molecules. The inset is a digital photo of bp-SNA/ITO before (right) and after confinement of MB molecules (left). CV curves of (B) MB@n-SNA/ITO and (C) MB@bp-SNA/ITO in 0.01 M PBS (pH = 7.4) during different times. The scan rate for CV tests in (B, C) is 50 mV/s.

electrostatic repulsion effect. Meanwhile, such MB@bp-SNA attached to the ITO electrode, termed as MB@bp-SNA/ITO, remains an open channel for effective mass transport and can be used for the construction of gate-controlled immunosensors for CA19-9 detection. CA19-9 antibody (Ab) as a recognition element is modified onto the top surface of bp-SNA with the help of the glutaraldehyde (GA) coupling agent. Ab/GA/MB@bp-SNA/ITO with specifically recognized capacity can be achieved after the blockage of nonspecific sites using bovine serum albumin (BSA). When target CA19-9 specifically interacts with the CA19-9 antibody to produce an antibody−antigen immunocomplex onto the Ab/GA/MB@bp-SNA/ITO electrode surface, the entrance of electrolyte ions through silica nanochannels to maintain charge balance is hampered and leads to the diminished electrochemical response of MB, finally realizing the quantitative determination of CA19-9.

3.2. Characterization of bp-SNA. Figure 1 shows the top-view TEM (A) and cross-sectional view SEM (B) images of bp-SNA. The as-prepared bp-SNA is composed of numerous nanoscale silica nanopores in a hexagonal arrangement (Figure 1A). In addition, the diameter of silica pores is uniform and about 2−3 nm. It could be found that bp-SNA consisting of two homogeneous layers, namely, p-SNA layer and n-SNA layer, is positioned on the top of ITO-coated glass

https://doi.org/10.1021/acsomega.3c08370
ACS Omega 2023, 8, 48491−48498

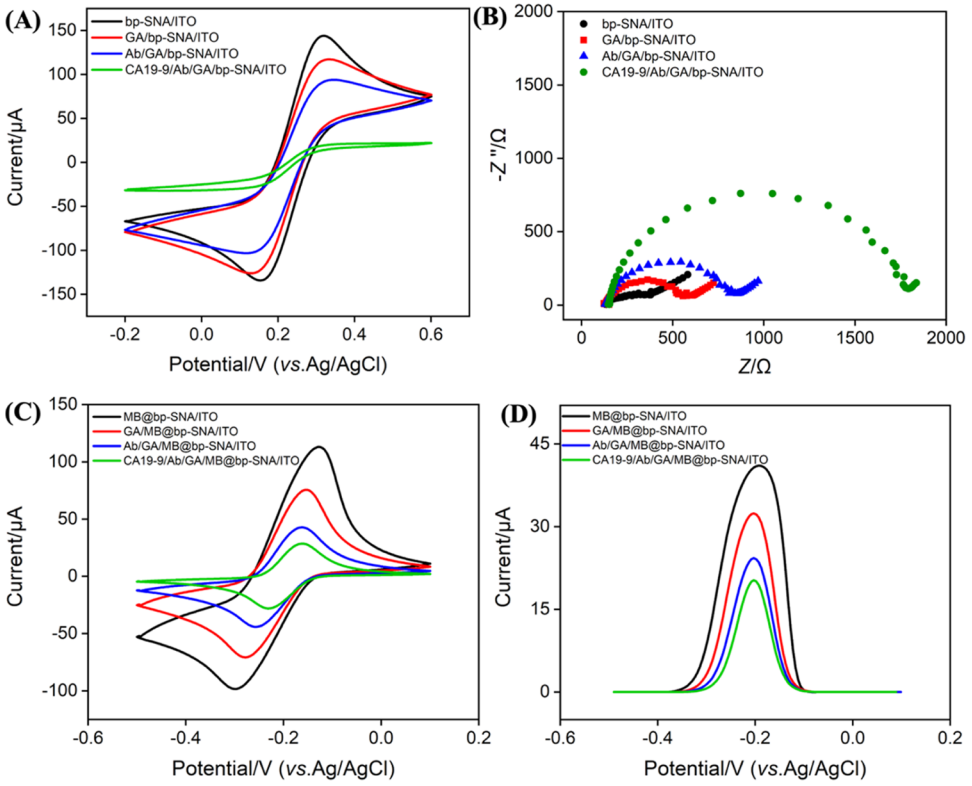

Figure 4. (A) CV and (B) EIS curves recorded with the stepwise modification electrodes. The electrolyte solution is 0.1 M KCl solution containing 2.5 mM $K_3[Fe(CN)_6]/K_4[Fe(CN)_6]$ (1: 1). (C) CV and (D) DPV curves of stepwise modification electrodes in 0.01 M PBS (pH = 7.4) at a potential scan from −0.5 to 0.1 V. The scan rate for CV tests in (A) and (C) is 50 mV/s.

(Figure 1B). p-SNA and n-SNA contain 92 and 78 nm length channel, respectively. As bp-SNA has opposite surface charges, the overall charge permselectivity of bp-SNA is studied by using two different charged reversible electrochemical redox, namely, $Fe(CN)_6^{3-}$ and MB. As shown in Figure 2, the n-SNA/ITO electrode displays electrostatic permselectivity, repulsing the ingress of $Fe(CN)_6^{3-}$ and attracting that of MB, compared to the bare ITO electrode. Compared to that of the n-SNA/ITO electrode, enhanced redox peak currents for $Fe(CN)_6^{3-}$ and decreased redox peak currents for MB are found at the bp-SNA/ITO, which is due to the suppression effect of the positively charged outer p-SNA layer. It is interesting that positively charged MB molecules can ignore the electrostatic repulsion effect by the outer p-SNA layer through mechanical stirring and be attracted by the inner n-SNA layer. After mechanical stirring for 10 min, MB can be stably confined into the inner nanospace of bp-SNA. However, the electrochemical response of $Fe(CN)_6^{3-}$ has no significant variation even under stirring for 30 min. These results suggest that the surface charge of the inner n-SNA layer plays an important role for overall charge permselectivity of the bipolar SNA membrane and the fabricated bp-SNA indeed has the capacity for electrostatic enrichment of MB molecules.

3.3. Stable Confinement of bp-SNA for MB. As shown in Figure S1, the MB molecule has two characteristic adsorption peaks around 600 and 650 nm, which are assigned to the dimer and monomer of MB, respectively.

Figure 3A shows the UV−vis spectra of the bp-SNA/ITO and MB@bp-SNA/ITO electrodes. As displayed, an obvious adsorption peak around at 600 nm and a weak adsorption peak around at 650 nm are observed at the MB@bp-SNA/ITO electrode, which is assigned to the MB molecules. From the photograph shown in the inset of Figure 3A, the MB@bp-SNA/ITO electrode clearly exhibits a blue color, suggesting the successful immobilization of MB molecules.

To evaluate the stabilization effect of bp-SNA for MB molecules, both bp-SNA/ITO and n-SNA/ITO were used to confine MB, to obtain MB@bp-SNA/ITO and MB@n-SNA/ITO electrodes, respectively. CV signals of MB@n-SNA/ITO and MB@bp-SNA/ITO electrodes in 0.01 M PBS (pH 7.4) at various times are recorded in Figure 3B,C. Within 25 min, electrochemical redox currents of MB diminish apparently at MB@n-SNA/ITO, whereas nearly no variation is found at MB@bp-SNA/ITO, revealing that the as-prepared MB@bp-SNA/ITO sensor has excellent stability and potential for long-term use. This is because bp-SNA emerged as an electrostatic nanocage that provides dual-force impact for cationic MB molecules, namely, electrostatic repulsion of the outer p-SNA layer and electrostatic preconcentration of the inner n-SNA layer.

3.4. Fabrication of the Ab/GA/MB@bp-SNA/ITO Immunosensor. To confirm that each modification step of Ab/GA/MB@bp-SNA/ITO is successful, CV and electrochemical impedance spectroscopy (EIS) were performed. bp-SNA/ITO without the confinement of MB was subjected to the prepared immunosensing interface and investigated by using the $Fe(CN)_6^{3-/4-}$ redox probe. Figure 4A shows the CV curves of bp-SNA/ITO, GA/bp-SNA/ITO, Ab/GA/bp-SNA/ITO, and CA19-9/Ab/GA/bp-SNA/ITO electrodes in 0.1 M KCl solution containing $Fe(CN)_6^{3-/4-}$. As seen, in comparison with the bp-SNA/ITO electrode, the voltammetric signal intensity of $Fe(CN)_6^{3-/4-}$ gradually decreases with the subsequent modification with GA or CA19-9 antibody, suggesting their successful immobilization. When Ab/GA/bp-

https://doi.org/10.1021/acsomega.3c08370
ACS Omega 2023, 8, 48491−48498

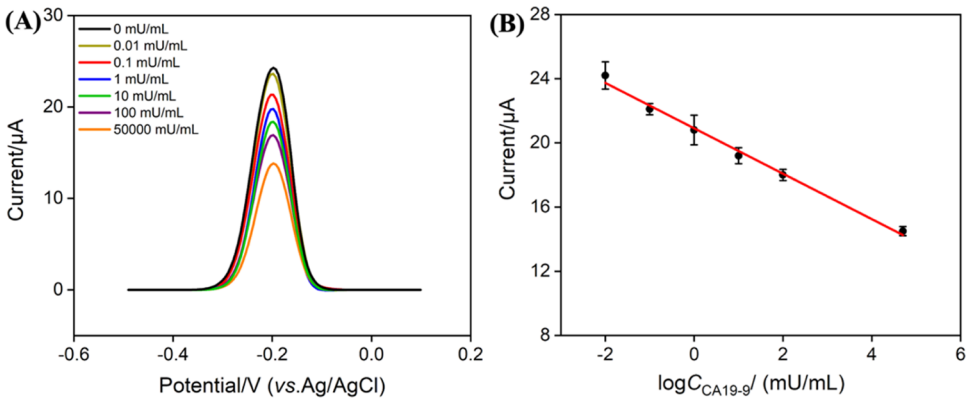

Figure 5. (A) DPV responses from continuous increases of CA19-9 amount into 0.01 M PBS (pH = 7.4) at the Ab/GA/MB@bp-SNA/ITO immunosensor. The concentrations of CA19-9 are 10 μU/mL, 100 μU/mL, 1 mU/mL, 10 mU/mL, 100 mU/mL, and 50 U/mL. (B) Calibration curve for CA19-9 detection using the fabricated Ab/GA/MB@bp-SNA/ITO electrode.

Table 1. Comparison of the Analytical Performances of Electrochemical Sensors for CA19-9 Determination

method	electrode	construction method	linear range (mU/mL)	LOD (mU/mL)	ref
ECL-RET	GO/HBP/ITO	labeled	$2-5 \times 10^4$	0.25	32
ECL	PtRu-PL-Ab_2/CA19-9/Ab_1/Au/GCE	labeled	$0.1-7 \times 10^4$	0.033	33
EIS	CeO_2/FeOx@mC500/AuE	label-free	$0.1-1 \times 10^4$	0.01	34
DPV	Au Ag HNCs/GCE	labeled	$1 \times 10^3-3 \times 10^4$	228	35
DPV	Ab/GA/MB@bp-SNA/ITO	label-free	$0.01-5 \times 10^4$	0.003	this work

RET: resonance energy transfer; GO/HBP: GO-grafted hyperbranched/aromaticpolyamide; PL: polylysines; CeO_2/FeOx@mC500: bimetallic cerium and ferric oxide nanoparticles embedded within the mesoporous carbon matrix; GCE: glassy carbon electrode; Au Ag HNCs: bimetallic alloyed Au Ag hollow nanocrystals.

SNA/ITO interacts with target CA19-9, the voltammetric signal intensity of $Fe(CN)_6^{3-/4-}$ apparently decreases, which arises from the steric hindrance effect of the CA19-9 antibody−antigen immunocomplex for $Fe(CN)_6^{3-/4-}$ and indicates the occurrence of specific recognition. In addition, functionalization of GA or CA19-9 antibody and interaction with CA19-9 can give rise to the enhanced charge transfer resistance (diameter of semicircles at high frequencies) (Figure 4B). In addition, CA19-9 antibody was labeled with fluorescent FITC molecules to obtain FITC-labeled CA19-9 antibody (FITC-Ab), which was used to modify the GA/bp-SNA/ITO or bp-SNA/ITO under the same experimental conditions. As shown in Figure S2 FITC-Ab/GA/bp-SNA/ITO displays the green fluorescence compared with Ab/GA/bp-SNA/ITO (Figures S2A,B), confirming the successful immobilization of CA19-9 antibody on the GA/bp-SNA/ITO electrode surface. By comparison, bp-SNA/ITO was used to incubate with CA19-9 antibody without the use of the GA coupling agent. No green fluorescence was observed (Figure 2C), further suggesting the important step of GA modification.

Due to the inherent redox characteristic of MB, MB@bp-SNA/ITO, GA/MB@bp-SNA/ITO, Ab/GA/MB@bp-SNA/ITO, and CA19-9/Ab/GA/MB@bp-SNA/ITO electrodes were soaked in 0.01 M PBS (pH 7.4) and tested for their electrochemical signals. As shown in Figure 4C,D, a pair of well-defined reversible redox peaks is obviously observed at MB@bp-SNA/ITO, corresponding to the electrochemical reaction of MB molecules electrostatically immobilized in the silica nanochannels of bp-SNA. Covalent modification of GA and CA19-9 antibody leads to the decreased redox peak current, and the addition of CA19-9 further generates the depleted current signals, indicating that our proposed Ab/GA/MB@bp-SNA/ITO sensing interface enables the quantitative determination of CA19-9.

3.5. Sensitive Response of the Developed Ab/GA/MB@bp-SNA/ITO Immunosensor for CA19-9 Detection. The analytical ability of the Ab/GA/MB@bp-SNA/ITO immunosensor was validated by incubation with the successively added concentrations of CA19-9 and tested in 0.01 M pure buffer (PBS, pH 7.4) using the DPV method. As presented in Figure 5, DPV responses decrease with the increasing CA19-9 amount, showing a proportional relationship between anodic peak current (I) and logarithm of concentration of CA19-9 ($\log C_{CA19\text{-}9}$) within a concentration range of 10 μU/mL to 50 U/mL. The acquired fitting linear regression equation and limit of detection (LOD) are I (μA) = $-1.41 \log C_{CA19\text{-}9} + 20.9$ ($R^2 = 0.996$) and 3 μU/mL (S/N = 3), respectively. The analytical performances of our as-prepared Ab/GA/MB@bp-SNA/ITO immunosensor studied in this work include the construction method, linear range, and LOD, which have been compared with those of other electrochemical sensors for CA19-9 determination, as shown in Table 1. The linear dynamic range obtained at our proposed Ab/GA/MB@bp-SNA/ITO immunosensor is wide, as well as a low LOD and simple fabrication procedure.

3.6. Interference of Coexisting Species on the Response of the Developed Ab/GA/MB@bp-SNA/ITO Immunosensor. The selectivity property of the developed Ab/GA/MB@bp-SNA/ITO immunosensor was assessed by measuring the electrochemical responses of 1 U/mL CA19-9 before (I_0) and after (I) the addition of potentially existing interfering substances. As shown in Figure 6, the obtained current ratio ($(I_0-I)/I_0$) is almost zero for the S100 calcium binding protein (S100), carcinoembryonic antigen (CEA), carcinoma antigen 125 (CA125), and bone γ-carboxyglutamate

https://doi.org/10.1021/acsomega.3c08370
ACS Omega 2023, 8, 48491−48498

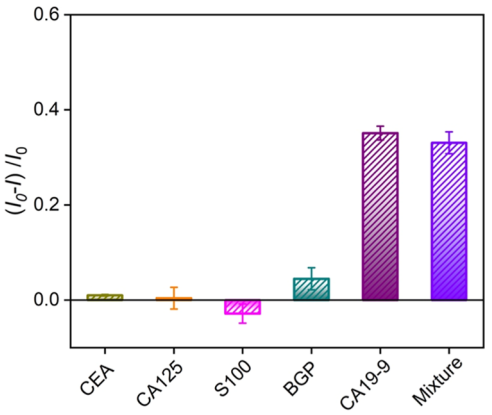

Figure 6. Selectivity of Ab/GA/MB@bp-SNA/ITO for the detection of CA19-9. The concentrations of CEA, S100, and BGP are 1 ng/mL, and those of CA125 and CA19-9 are 1 U/mL.

protein (BGP). However, the presence of CA19-9 or mixture consisting of CA19-9 and four other interfering substances can produce available signals, indicating the good selectivity of the Ab/GA/MB@bp-SNA/ITO immunosensor for CA19-9 detection. In addition, arising from the inherent property of silica, the fabricated Ab/GA/MB@bp-SNA/ITO immunosensor is not fit for quantitative analysis in strong alkaline media. However, CA19-9 often exists in human serum and its amount can be tested by our immunosensor.

3.7. Detection of CA19-9 in Human Serum. The antifouling detection ability of the developed Ab/GA/MB@bp-SNA/ITO immunosensor was studied by using a biological complex matrix (human serum). Directly obtained human serum samples were only diluted by 0.01 M PBS (pH 7.4) without other tedious pretreatments, which were then tested by the Ab/GA/MB@bp-SNA/ITO immunosensor. No obvious electrochemical signal was observed. After being spiked with a series of CA19-9 with known concentrations, human samples were tested with our fabricated Ab/GA/MB@bp-SNA/ITO immunosensor. Table 2 lists the measured (found) and spiked concentrations. It could be found that the achieved recoveries are from 96.0 to 102% with relatively low RSD (less than 4.5%) and imply the great practical ability of the Ab/GA/MB@bp-SNA/ITO immunosensor.

Table 2. Recoveries of CA19-9 in Spiked Human Serum Samples[a]

media	added (U/mL)	found (U/mL)	recovery (%)	RSD (%)
human serum[a]	0.00100	0.00100	100	2.1
	1.00	0.968	96.0	4.5
	50.0	51.1	102	3.8

[a]Samples were diluted by 50-fold buffer solution and then detected by our fabricated sensor.

4. CONCLUSIONS

In summary, bp-SNA consisting of n-SNA and p-SNA was employed for confinement and enrichment of MB molecules into the inner layer and further construction of the probe-integrated electrochemical immunosensor for CA19-9 detection. bp-SNA served as a solid substrate and can not only confine and preconcentrate redox-active MB molecules inside the silica nanochannels to generate amplified and stable electrochemical signal but also render functional sites for covalent immobilization of CA19-9 antibody to specifically recognize CA19-9. By recording the electrochemical signals of the proposed electrochemical immunosensor upon the capture of CA19-9, reagentless determination of CA19-9 is realized with a wide linear dynamic range and a low LOD. The potential clinical utility of our proposed electrochemical immunosensor in complex human serum is also demonstrated with satisfactory results. The present strategy may be useful in the development of probe-integrated electrochemical immunosensors and could be extended to directly analyze CA19-9 in clinical applications and point-of-care diagnostics.

■ ASSOCIATED CONTENT

Supporting Information

The Supporting Information is available free of charge at https://pubs.acs.org/doi/10.1021/acsomega.3c08370.

Detailed experimental section; UV−vis characterization of the MB molecule and fluorescence characterization of immobilized CA19-9 antibody (PDF)

■ AUTHOR INFORMATION

Corresponding Authors

Fei Yan − *Key Laboratory of Surface & Polymer Materials of Zhejiang Province, Department of Chemistry, School of Chemistry and Chemical Engineering, Zhejiang Sci-Tech University, Hangzhou 310018, China;* orcid.org/0000-0002-2822-698X; Email: yanfei@zstu.edu.cn

Yiping Mou − *Medical College of Soochow University, Suzhou 215006, China; General Surgery, Cancer Center, Department of Gastrointestinal and Pancreatic Surgery, Zhejiang Provincial People's Hospital, Hangzhou Medical College, Hangzhou 310014, China;* Email: yipingmou@126.com

Authors

Yucheng Zhou − *Medical College of Soochow University, Suzhou 215006, China; General Surgery, Cancer Center, Department of Gastrointestinal and Pancreatic Surgery, Zhejiang Provincial People's Hospital, Hangzhou Medical College, Hangzhou 310014, China*

Xuan Luo − *Key Laboratory of Surface & Polymer Materials of Zhejiang Province, Department of Chemistry, School of Chemistry and Chemical Engineering, Zhejiang Sci-Tech University, Hangzhou 310018, China*

Complete contact information is available at: https://pubs.acs.org/10.1021/acsomega.3c08370

Notes

The authors declare no competing financial interest.

■ ACKNOWLEDGMENTS

This study was funded by the Zhejiang Provincial Natural Science Foundation of China (LGF20H160011 and LY21B050003) and the Fundamental Research Funds of Zhejiang Sci-Tech University (22062310-Y).

■ REFERENCES

(1) Chen, H. F.; Gao, Z. Q.; Cui, Y. L.; Chen, G. N.; Tang, D. P. Nanogold-Enhanced Graphene Nanosheets as Multienzyme Assembly for Sensitive Detection of Low-Abundance Proteins. *Biosens. Bioelectron.* **2013**, *44*, 108−114.

(2) Jawad, Z. A. R.; Theodorou, I. G.; Jiao, L. R.; Xie, F. Highly Sensitive Plasmonic Detection of the Pancreatic Cancer Biomarker Ca 19-9. *Sci. Rep.* **2017**, *7*, No. 14309, DOI: 10.1038/s41598-017-14688-z.
(3) Su, C. W.; Tian, J. H.; Ye, J. J.; Chang, H. W.; Tsai, Y. C. Construction of a Label-Free Electrochemical Immunosensor Based on Zn-Co-S/Graphene Nanocomposites for Carbohydrate Antigen 19-9 Detection. *Nanomaterials* **2021**, *11* (6), No. 1475, DOI: 10.3390/nano11061475.
(4) Humphris, J. L.; Chang, D. K.; Johns, A. L.; Scarlett, C. J.; Pajic, M.; Jones, M. D.; Colvin, E. K.; Nagrial, A.; Chin, V. T.; Chantrill, L. A.; Samra, J. S.; Gill, A. J.; Kench, J. G.; Merrett, N. D.; Das, A.; Musgrove, E. A.; Sutherland, R. L.; Biankin, A. V.; NSW Pancreatic Cancer Network. The Prognostic and Predictive Value of Serum Ca19.9 in Pancreatic Cancer. *Ann. Oncol.* **2012**, *23* (7), 1713−1722, DOI: 10.1093/annonc/mdr561.
(5) Heidari, M. H.; Porghasem, M.; Mirzaei, N.; Mohseni, J. H.; Heidari, M.; Azargashb, E.; Movafagh, A.; Heidari, R.; Molouki, A.; Larijani, L. The Effect of High Level Natural Ionizing Radiation on Expression of Psa, Ca19-9 and Cea Tumor Markers in Blood Serum of Inhabitants of Ramsar, Iran. *J. Environ. Radioact.* **2014**, *128*, 64−67.
(6) Gu, B. X.; Xu, C. X.; Yang, C.; Liu, S. Q.; Wang, M. L. Zno Quantum Dot Labeled Immunosensor for Carbohydrate Antigen 19-9. *Biosens. Bioelectron.* **2011**, *26* (5), 2720−2723.
(7) Shi, M.; Zhao, S. L.; Huang, Y.; Zhao, L. M.; Liu, Y. M. Signal Amplification in Capillary Electrophoresis Based Chemiluminescent Immunoassays by Using an Antibody-Gold Nanoparticle-Dnazyme Assembly. *Talanta* **2014**, *124*, 14−20.
(8) Ma, K.; Zheng, Y. Y.; An, L. Z.; Liu, J. Y. Ultrasensitive Immunosensor for Prostate-Specific Antigen Based on Enhanced Electrochemiluminescence by Vertically Ordered Mesoporous Silica-Nanochannel Film. *Front. Chem.* **2022**, *10*, No. 851178, DOI: 10.3389/fchem.2022.851178.
(9) Yan, L.; Zhang, C. Y.; Xi, F. N. Disposable Amperometric Label-Free Immunosensor on Chitosan-Graphene-Modified Patterned Ito Electrodes for Prostate Specific Antigen. *Molecules* **2022**, *27* (18), No. 5895, DOI: 10.3390/molecules27185895.
(10) Lin, J.; Li, K. Y.; Wang, M. F.; Chen, X. H.; Liu, J. Y.; Tang, H. L. Reagentless and Sensitive Determination of Carcinoembryonic Antigen Based on a Stable Prussian Blue Modified Electrode. *RSC Adv.* **2020**, *10* (63), 38316−38322.
(11) Zhang, J.; Yang, L. X.; Pei, J.; Tian, Y. Z.; Liu, J. Y. A Reagentless Electrochemical Immunosensor for Sensitive Detection of Carcinoembryonic Antigen Based on the Interface with Redox Probe-Modified Electron Transfer Wires and Effectively Immobilized Antibody. *Front. Chem.* **2022**, *10*, No. 939736, DOI: 10.3389/fchem.2022.939736.
(12) Chang, Q.; Huang, J.; He, L. M.; Xi, F. N. Simple Immunosensor for Ultrasensitive Electrochemical Determination of Biomarker of the Bone Metabolism in Human Serum. *Front. Chem.* **2022**, *10*, No. 940795, DOI: 10.3389/fchem.2022.940795.
(13) Deng, X. C.; Lin, X. T.; Zhou, H. X.; Liu, J. Y.; Tang, H. L. Equipment of Vertically-Ordered Mesoporous Silica Film on Electrochemically Pretreated Three-Dimensional Graphene Electrodes for Sensitive Detection of Methidazine in Urine. *Nanomaterials* **2023**, *13* (2), No. 239, DOI: 10.3390/nano13020239.
(14) Zheng, W. R.; Su, R. B.; Lin, X. Y.; Liu, J. Y. Nanochannel Array Modified Three-Dimensional Graphene Electrode for Sensitive Electrochemical Detection of 2,4,6-Trichlorophenol and Prochloraz. *Front. Chem.* **2022**, *10*, No. 954802, DOI: 10.3389/fchem.2022.954802.
(15) Zhou, H. X.; Ding, Y.; Su, R. B.; Lu, D. M.; Tang, H. L.; Xi, F. N. Silica Nanochannel Array Film Supported by Ss-Cyclodextrin-Functionalized Graphene Modified Gold Film Electrode for Sensitive and Direct Electroanalysis of Acetaminophen. *Front. Chem.* **2022**, *9*, No. 812086, DOI: 10.3389/fchem.2021.812086.
(16) Zhu, X. Q.; Xuan, L. L.; Gong, J. W.; Liu, J. J.; Wang, X. B.; Xi, F. N.; Chen, J. Three-Dimensional Macroscopic Graphene Supported Vertically-Ordered Mesoporous Silica-Nanochannel Film for Direct and Ultrasensitive Detection of Uric Acid in Serum. *Talanta* **2022**, *238*, No. 123027, DOI: 10.1016/j.talanta.2021.123027.
(17) Lv, N.; Qiu, X.; Han, Q. Q.; Xi, F. N.; Wang, Y.; Chen, J. Anti-Biofouling Electrochemical Sensor Based on the Binary Nanocomposite of Silica Nanochannel Array and Graphene for Doxorubicin Detection in Human Serum and Urine Samples. *Molecules* **2022**, *27* (24), No. 8640, DOI: 10.3390/molecules27248640.
(18) Ma, K.; Yang, L. X.; Liu, J.; Liu, J. Y. Electrochemical Sensor Nanoarchitectonics for Sensitive Detection of Uric Acid in Human Whole Blood Based on Screen-Printed Carbon Electrode Equipped with Vertically-Ordered Mesoporous Silica-Nanochannel Film. *Nanomaterials* **2022**, *12* (7), No. 1157, DOI: 10.3390/nano12071157.
(19) Zhou, H. X.; Ma, X. Y.; Sailjoi, A.; Zou, Y. Q.; Lin, X. Y.; Yan, F.; Su, B.; Liu, J. Y. Vertical Silica Nanochannels Supported by Nanocarbon Composite for Simultaneous Detection of Serotonin and Melatonin in Biological Fluids. *Sens. Actuators, B* **2022**, *353*, No. 131101, DOI: 10.1016/j.snb.2021.131101.
(20) Zhou, P.; Yao, L. N.; Chen, K. X.; Su, B. Silica Nanochannel Membranes for Electrochemical Analysis and Molecular Sieving: A Comprehensive Review. *Crit. Rev. Anal. Chem.* **2020**, *50* (5), 424−444.
(21) Zhou, L.; Hou, H.; Wei, H.; Yao, L.; Sun, L.; Yu, P.; Su, B.; Mao, L. In Vivo Monitoring of Oxygen in Rat Brain by Carbon Fiber Microelectrode Modified with Antifouling Nanoporous Membrane. *Anal. Chem.* **2019**, *91* (5), 3645−3651.
(22) Su, R. B.; Tang, H. L.; Xi, F. N. Sensitive Electrochemical Detection of P-Nitrophenol by Pre-Activated Glassy Carbon Electrode Integrated with Silica Nanochannel Array Film. *Front. Chem.* **2022**, *10*, No. 954748, DOI: 10.3389/fchem.2022.954748.
(23) Huang, L. Y.; Su, R. B.; Xi, F. N. Sensitive Detection of Noradrenaline in Human Whole Blood Based on Au Nanoparticles Embedded Vertically-Ordered Silica Nanochannels Modified Pre-Activated Glassy Carbon Electrodes. *Front. Chem.* **2023**, *11*, No. 1126213, DOI: 10.3389/fchem.2023.1126213.
(24) Huang, J.; Zhang, T. T.; Zheng, Y. Y.; Liu, J. Y. Dual-Mode Sensing Platform for Cancer Antigen 15−3 Determination Based on a Silica Nanochannel Array Using Electrochemiluminescence and Electrochemistry. *Biosensors* **2023**, *13* (3), No. 317, DOI: 10.3390/bios13030317.
(25) Zhou, X.; Han, Q.; Zhou, J.; Liu, C.; Liu, J. Reagentless Electrochemical Detection of Tumor Biomarker Based on Stable Confinement of Electrochemical Probe in Bipolar Silica Nanochannel Film. *Nanomaterials* **2023**, *13* (10), No. 1645, DOI: 10.3390/nano13101645.
(26) Yan, L.; Xu, S.; Xi, F. N. Disposal Immunosensor for Sensitive Electrochemical Detection of Prostate-Specific Antigen Based on Amino-Rich Nanochannels Array-Modified Patterned Indium Tin Oxide Electrode. *Nanomaterials* **2022**, *12* (21), No. 3810, DOI: 10.3390/nano12213810.
(27) Ding, H.; Guo, W. L.; Zhou, P.; Su, B. Nanocage-Confined Electrochemiluminescence for the Detection of Dopamine Released from Living Cells. *Chem. Commun.* **2020**, *56* (59), 8249−8252.
(28) Gong, J. W.; Zhang, T. T.; Luo, T.; Luo, X.; Yan, F.; Tang, W. Z.; Liu, J. Y. Bipolar Silica Nanochannel Array Confined Electrochemiluminescence for Ultrasensitive Detection of Sars-Cov-2 Antibody. *Biosens. Bioelectron.* **2022**, *215*, No. 114563, DOI: 10.1016/j.bios.2022.114563.
(29) Gong, J. W.; Zhang, T. T.; Chen, P.; Yan, F.; Liu, J. Y. Bipolar Silica Nanochannel Array for Dual-Mode Electrochemiluminescence and Electrochemical Immunosensing Platform. *Sens. Actuators, B* **2022**, *368*, No. 132086, DOI: 10.1016/j.snb.2022.132086.
(30) Cui, L.; Lu, M. F.; Li, Y.; Tang, B.; Zhang, C. Y. A Reusable Ratiometric Electrochemical Biosensor on the Basis of the Binding of Methylene Blue to DNA with Alternating at Base Sequence for Sensitive Detection of Adenosine. *Biosens. Bioelectron.* **2018**, *102*, 87−93.
(31) Schoukroun-Barnes, L. R.; Macazo, F. C.; Gutierrez, B.; Lottermoser, J.; Liu, J.; White, R. J. Reagentless, Structure-Switching,

Electrochemical Aptamer-Based Sensors. *Annu. Rev. Anal. Chem.* **2016**, *9*, 163−181.
(32) Bahari, D.; Babamiri, B.; Salimi, A.; Hallaj, R.; Amininasab, S. M. A Self-Enhanced Ecl-Ret Immunosensor for the Detection of Ca19-9 Antigen Based on $Ru(Bpy)_2(Phen\text{-}Nh_2)^{2+}$ - Amine-Rich Nitrogen-Doped Carbon Nanodots as Probe and Graphene Oxide Grafted Hyperbranched Aromatic Polyamide as Platform. *Anal. Chim. Acta* **2020**, *1132*, 55−65.
(33) Tan, Y.-Y.; Sun, H.-N.; Liu, M.; Liu, A.; Li, S.-S. Simple Synthesis of Ptru Nanoassemblies as Signal Amplifiers for Electrochemical Immunoassay of Carbohydrate Antigen 19-9. *Bioelectrochemistry* **2022**, *148*, No. 108263.
(34) Wang, M.; Hu, M.; Hu, B.; Guo, C.; Song, Y.; Jia, Q.; He, L.; Zhang, Z.; Fang, S. Bimetallic Cerium and Ferric Oxides Nanoparticles Embedded within Mesoporous Carbon Matrix: Electrochemical Immunosensor for Sensitive Detection of Carbohydrate Antigen 19-9. *Biosens. Bioelectron.* **2019**, *135*, 22−29.
(35) Wang, R.; Feng, J.; Liu, W.; Jiang, L.; Wang, A. A Novel Label-Free Electrochemical Immunosensor Based on the Enhanced Catalytic Currents of Oxygen Reduction by Auag Hollow Nanocrystals for Detecting Carbohydrate Antigen 199. *Biosens. Bioelectron.* **2017**, *96*, 152−158.

https://doi.org/10.1021/acsomega.3c08370
ACS Omega 2023, 8, 48491−48498